

A dynamically tunable and wide-angle terahertz absorber based on graphene-dielectric grating

Chunyan Wu, Yiqiang Fang and Linbao Luo*

*School of Electronic Science and Applied Physics,
Hefei University of Technology, Hefei 230009, China*
*luolb@hfut.edu.cn

Kai Guo and Zhongyi Guo†

*School of Computer and Information,
Hefei University of Technology, Hefei 230601, China*
†guozhongyi@hfut.edu.cn

Received 21 January 2020

Revised 7 March 2020

Accepted 10 March 2020

Published 1 July 2020

We theoretically and numerically demonstrate a tunable and wide-angle terahertz absorber, which is composed of multilayer graphene-dielectric grating and bottom metal substrate. Numerical simulation shows that the proposed absorber has the advantage of dynamically tunable range from 1.015 THz to 1.165 THz when the chemical potential of graphene increases from 10 meV to 150 meV. The absorption efficiency can reach a high value of 99%. To show the working mechanism of absorption, the near field distributions of magnetic components are presented at the absorption wavelength. We also demonstrate that the tunable range of absorption can be engineered by designing the geometry parameters. In addition, it is shown that the designed absorber can maintain the good performance of absorption over a wide incident angle from 0° to 60° under TM-polarization.

Keywords: Tunable absorber; terahertz; graphene.

1. Introduction

Terahertz generally refers to electromagnetic waves with a frequency in 0.1–10 terahertz band, which is in the transition region from macro-classical theory to micro-quantum theory and from electronics to photonics. Many functions such as imaging, radar, and communication are being extensively studied in the terahertz region.^{1,2} Recently, there are a series of works to achieve perfect absorption in terahertz range with subwavelength scale units,³ which are widely used in the various fields, such as biomedical and molecular detection owing to their advantages

†Corresponding author.

of small size and easy integration. A popular construction of perfect absorbers (PAs) is based on metal-insulator-metal (MIM) plasmonic structures. By optimally adjusting the geometrical parameters and composite materials, impedance matching between free space and MIM structure can be achieved, forming perfect absorption spectrum.^{4–6} Lee *et al.* designed an one-dimensional sandwiched absorber structure which employs a Fabry–Pérot resonance cavity to obtain sharp absorption peak.⁷ With the development of plasmonic PAs, researchers began to be dissatisfied with the single absorbing band since the resonance frequency is fixed after the designing of PAs. Therefore, researches moved to study the multiple bands⁸ and wide band absorbers,^{9,10} by combing several electromagnetic resonances,^{11,12} and tunable terahertz absorbers by utilizing active materials.¹³

Among all these active materials, graphene is regarded as a promising candidate for plasmonic material due to its excellent properties, especially the dynamical tunable conductivity and the atomical thickness.¹³ Consequently, tremendous research interests have been paid to introduce graphene to PAs to achieve tunable absorption performance.^{14–16} For instance, Chen *et al.* designed a broadband optical absorption structure to obtain broadband and reconfigurable absorption in terahertz through coupling between monolayer-graphene and periodic metal structure.¹⁷ In 2018, Rahmanzadeh *et al.* systematically designed a terahertz absorber based on multi-layer graphene-based metasurfaces by using an equivalent circuit method, providing an extremely broad absorption bandwidth and polarization-independent property for TE- and TM-polarizations due to its symmetrical structure.¹⁸ Akhavan *et al.* investigated PAs by employing guided mode resonance to realize highly efficient absorption of light in the graphene sheet.¹⁹ Wang *et al.* proposed graphene-based terahertz absorbers with tunable and multiband absorption peaks.^{20–22} It is also important for the absorbers to have applicability of large incident angle, which will be practical for the application of the devices. The above-mentioned works have achieved great performance of absorption by utilizing graphene layers.^{15–17,20–24}

In this paper, we designed a graphene-dielectric grating-based plasmonic absorber in terahertz region. The absorption frequency can be tuned from 1.015 THz to 1.165 THz by changing the chemical potential of graphene from 10 meV to 150 meV. The absorption efficiency can reach a high value of 99%. To investigate the physical nature of absorption, the near field distributions of magnetic components are studied at the absorption wavelength. It is also shown that the tunable range of absorption can be engineered by designing the geometry parameters. In addition, the designed absorber can maintain the good performance of the absorption over a wide incident angle from 0° to 60° under TM-polarization.

2. Results and Discussion

Figure 1 presents the schematic of the designed absorber, which is composed of periodic graphene-dielectric grating along x -axis and a metal ground plane. The period is $p = 140 \mu\text{m}$ and the graphene width is $w = p \times f = 63 \mu\text{m}$, in which

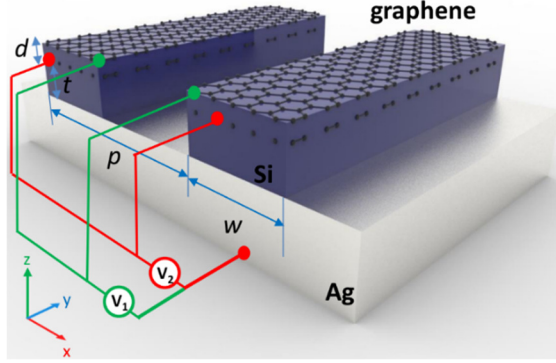


Fig. 1. Schematic of the proposed grating absorber based on periodic graphene-Si bilayers on Ag substrate. The structural parameters are $p = 140 \mu\text{m}$, $w = 63 \mu\text{m}$, $h = 0.0034 \mu\text{m}$, $d = 60 \mu\text{m}$ and $t = 40 \mu\text{m}$.

$f = 0.45$ is the duty cycle for the periodic grating. Along the y -axis, the device is regarded as infinite. The grating consists of two layers of graphene/Si dielectric stacking. The material of the metal ground plane is silver, which is thick enough to prevent transmitted light.

Two-dimensional simulations have been performed by using a home-built program based on finite-element method. The incident light is TM-polarized in infrared region with the incident angle of θ . The thickness of each graphene layer is chosen as $h = 3.4 \text{ nm}$, which is 10 times of monolayer graphene.^{25,26} It is to enhance the coupling between the graphene layers and the incident light, thereby, increasing the absorption effect of the graphene layers. The top and bottom Si layers are $d = 60 \mu\text{m}$ and $t = 40 \mu\text{m}$, respectively. Considering the skin depth of the silver, we set $s = 60 \mu\text{m}$ as the thickness of substrate.

The relative permittivity of silver (Ag) is described by a Drude model as follows²⁷:

$$\varepsilon_{\text{Ag}} = 1 - \frac{\omega_p^2}{\omega(\omega - i\gamma\omega)}, \quad (1)$$

where $\omega_p = 1.37036 \times 10^{16} \frac{\text{rad}}{\text{s}}$ and $\gamma = 1.71732 \times 10^{16} \frac{\text{rad}}{\text{s}}$ are the plasma frequency and damping frequency of silver, respectively. The permittivity of dielectric Si is set as a constant of $\varepsilon_{\text{Si}} = 11.7$ since the dispersion of Si in terahertz region is relatively negligible in comparison to silver and graphene.

The optical property of graphene layer is described by the conductivity σ_G which could be calculated according to the Kubo model.^{28,29} At finite temperatures, the conductivity can be divided into intra- and inter-band conductivity^{30,31}:

$$\sigma_G = \sigma_G^{\text{intra}} + \sigma_G^{\text{inter}}, \quad (2)$$

$$\sigma_G^{\text{intra}} = \frac{ie^2}{8\pi\hbar} \left\{ \frac{16k_B T}{\hbar(\omega + i\Gamma)} \ln \left[2 \cosh \left(\frac{\mu_c}{2k_B T} \right) \right] \right\}, \quad (3)$$

$$\sigma_G^{\text{inter}} = \frac{e^2}{4\hbar} \left\{ \frac{1}{2} + \frac{1}{\pi} \arctan \left(\frac{\hbar\omega - 2\mu_c}{2k_B T} \right) - \frac{i}{2\pi} \ln \left[\frac{(\hbar\omega + 2\mu_c)^2}{(\hbar\omega - 2\mu_c)^2 + (2k_B T)^2} \right] \right\}. \quad (4)$$

In Eqs. (3) and (4), e is the elementary charge, \hbar and k_B are the reduced Planck's constant and Boltzmann constant, respectively. ω is the angular frequency. T denotes the temperature and Γ indicates the scattering rate of charge carriers, which are chosen as 300 K and $2\pi \cdot 0.1$ meV/ \hbar , respectively. The chemical potential μ_c could be regulated by electrostatic fields through adding electric potential difference between graphene and silver grid.

$$\mu_c = \hbar v_f \sqrt{\pi \frac{\epsilon_{\text{Si}} \epsilon_0 V_b}{eh'}}, \quad (5)$$

where the Fermi speed is set as $v_f = 10^6$ m/s, V_b is the applied electric potential, value of h' is $d + t$ and t when the electric potential is applied at the upper and bottom graphene layers, respectively. In the way, the chemical potential μ_c and optical properties of graphene layers could be adjusted by varying external voltage. To ensure the same properties of two graphene layers, the ratio of external voltage applied at the upper graphene to that at the lower graphene is $(d + t)/t$.

To demonstrate the tunable performance of the designed absorber, Fig. 2(a) depicts the absorption spectrum as a function of chemical potential μ_c . There is an absorption peak at frequency of 1.015 THz for TM-polarization when $\mu_c = 10$ meV. When the chemical potential μ_c increases from 10 meV to 150 meV, the frequency of absorption peak blue shifts from 1.015 THz to 1.165 THz. In addition, the efficiency of absorption peaks reaches more than 95% during the range of chemical potential μ_c from 10 meV to 150 meV. The full width at half maximum (FWHM) of the peaks could maintains at a high level from 0.025 THz to 0.010 THz as μ_c increases from 10 meV to 150 meV, except for the frequencies around 60 meV. To investigate this effect, we extract the absorption spectra at chemical potential of 10, 60, 80 and 100 meV (marked with white dotted lines) and plot them in Fig. 2(b). Besides the main absorption peaks, minor absorption peaks can be observed at frequency around 1.1 THz and 1.2 THz for the cases of $\mu_c = 10$ meV and $\mu_c = 80$ meV, respectively.

The magnetic fields corresponding to absorption peaks with the serial number are depicted in Figs. 3(a)–3(f). The red arrows represent the current density. The results in Figs. 3(a)–3(d) have similar features that magnetic resonance can be induced by the circular distributed currents in either the upper or lower Si layer. It can be seen that the resonance in upper medium is caused by anti-parallel currents between the upper and lower graphene layers. In contrast, the resonance in lower medium is resulted from anti-parallel currents between the lower graphene layer and metal ground. For Figs. 3(e) and 3(f), besides of magnetic fields located in the medium above the metal plane, we can observe magnetic resonance localized at the upper and the bottom graphene layers, respectively. The spectral splitting in Fig. 2(a) around 60 meV is due to overlapping between the modes occurred in Fig. 3(f) and main mode represented by Fig. 3(d).

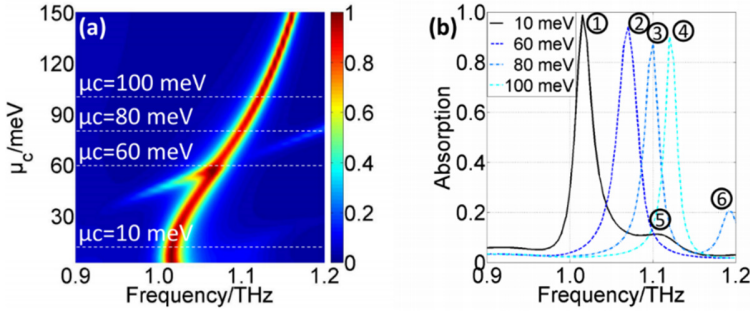


Fig. 2. (Color online) (a) The calculated absorption spectrum as a function of chemical potential μ_c of the proposed absorber for TM polarization at normal incidence and (b) absorption spectra taken from the white dotted line in (a).

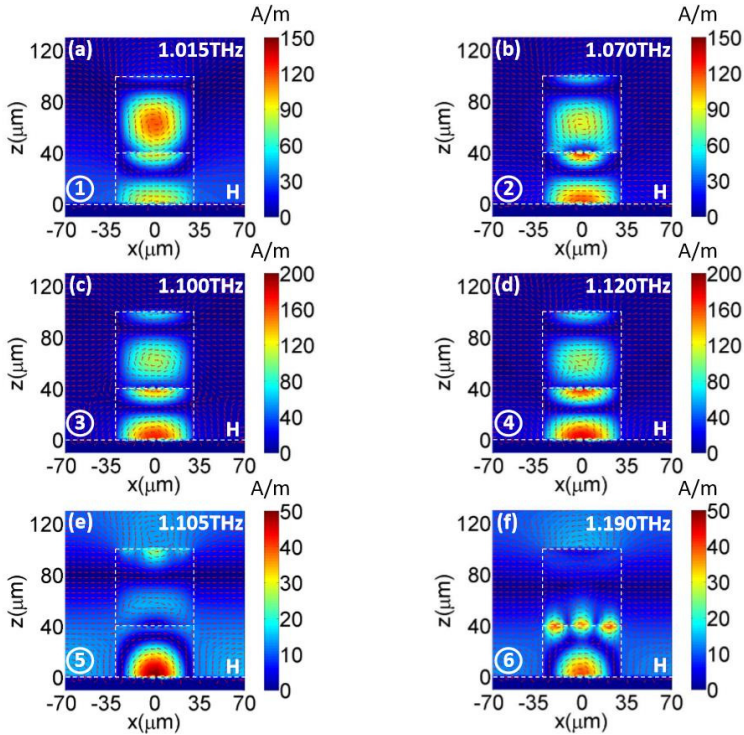


Fig. 3. (Color online) (a)–(f) Calculated magnetic fields at the absorption peaks marked with serial number 1 to 6 in Fig. 2(b). The red arrows represent the current density.

As well known, the working frequency of plasmonic structure is highly dependent on its geometry parameters. Therefore, we may have different tunable range of the proposed absorber by changing the geometry parameters. To investigate, the absorption spectrum is simulated as functions d , p , t and f , as shown in Fig. 4. In these cases, the chemical potential is fixed at $\mu_c = 10$ meV. It can be observed that

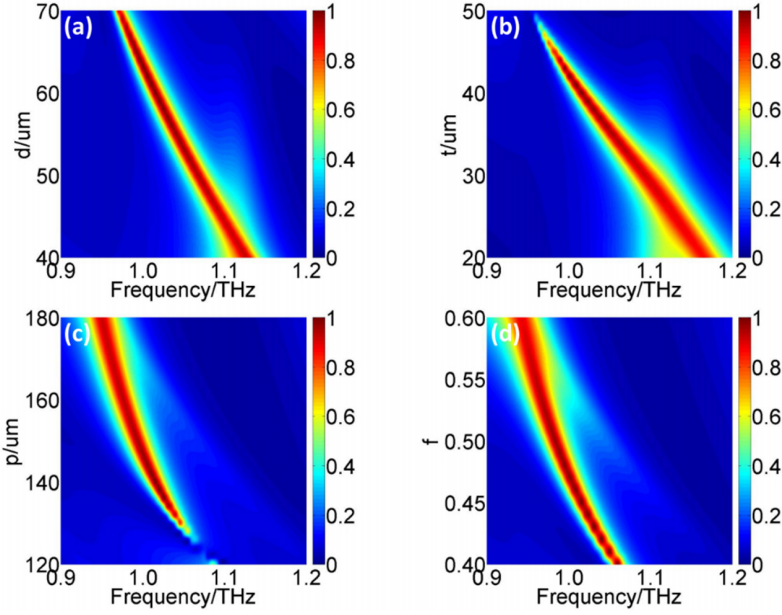


Fig. 4. (Color online) Absorption spectrum as a function of frequency and thickness of the top dielectric layer Si, thickness of the bottom dielectric layer Si, and grating period for TM polarization when μ_c is set as 10 meV. The structural parameters are: $\theta = 0^\circ$, $p = 140 \mu\text{m}$, $f = 0.45$, $w = p \times f = 63 \mu\text{m}$, $h = 0.0034 \mu\text{m}$, $d = 60 \mu\text{m}$ and $t = 40 \mu\text{m}$. In (a) d is varied from $40 \mu\text{m}$ to $70 \mu\text{m}$, in (b) t is varied from $20 \mu\text{m}$ to $50 \mu\text{m}$, in (c) p is varied from $120 \mu\text{m}$ to $180 \mu\text{m}$, and in (d) f is varied from 0.40 to 0.60.

the main absorption peaks move to lower frequency with the increasing of d , p , t and f , which can be explained by the equivalent circuit model.^{5,32–36} In this model, the plasmonic and dielectric composites can be treated as inductor and capacitor, respectively, and the eigen-frequency of the proposed absorber is $f_0 = \frac{1}{\sqrt{LC}}$. With the increasing of d , p and t , f , the value of inductance L and capacitance C will be increased, resulting in red shifts of the absorption peak. In addition, the simulation results show that bandwidths of absorption gradually reduce when d and t increase, or p and f decrease. The absorption intensities are almost above 85% and the absorption peak can move from 0.950 THz to 1.165 THz, which could be further tuned by applying external voltage. Besides, the minor absorption peak, shown in Fig. 3(e), overlaps with the main peaks, causing the bandwidths increasing in part regions, as can be seen Fig. 4.

A unique feature of absorber is insensitive to incident conditions. Therefore, the absorption spectrum is simulated as a function of angle of incidence θ , as shown in Fig. 5. When incident angle increases from 0° to 60° , the resonance peak slightly red shifts to the lower frequency, meanwhile, the bandwidth of absorption peak increases from 0.025 THz to 0.035 THz. At the same time, the value of absorption efficiency keeps at a high level over 75%. This can be understood from the physical

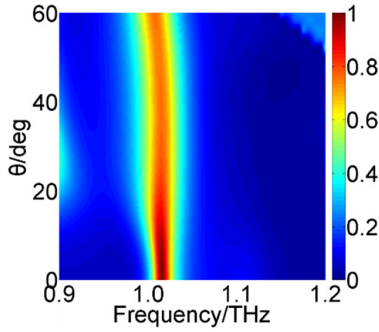


Fig. 5. (Color online) Absorption spectrum under the illumination of TM-polarized wave as a function of the incident angle θ range from 0° to 60° . The geometric parameters remain unchanged.

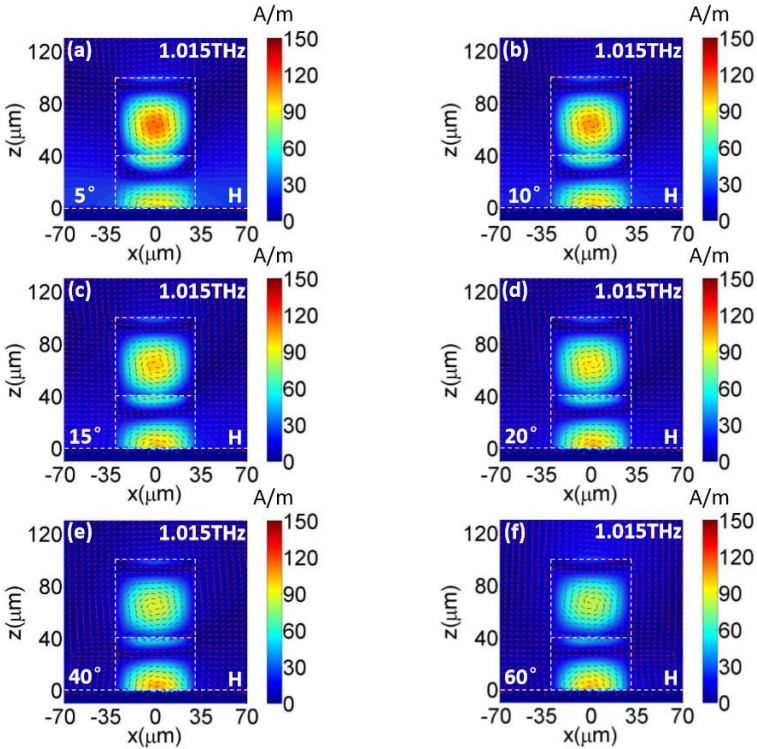


Fig. 6. (Color online) (a)–(f) Calculated magnetic fields at frequency of 1.015 THz under incident angle of 5° , 10° , 15° , 20° , 40° and 60° , respectively. The red arrows represent the current density.

nature of the absorption peak, which originates from magnetic resonances with high symmetry. Therefore, the absorption peak is almost independent on incident angle.

To show the performance of the proposed absorber, we calculated the near field distributions of the magnetic component and electric current at frequency of 1.015 THz under incident angle of 5° , 10° , 15° , 20° , 40° and 60° , as plotted in Fig. 6.

It can be seen that the field distributions possess the unique features of magnetic resonance. In addition, the field intensity maintains at a similar level. These results demonstrate further that the proposed absorber has a good angle adaptability which arises from the magnetic resonance. Overall, the designed absorber has excellent angular adaptability that the frequency and efficiency of absorption spectra remains stable for incident angles from 0° to 60° , indicating the great performance of our proposed terahertz absorber.

3. Conclusions

In summary, we designed a graphene-dielectric grating absorber in terahertz region, gaining properties of the tunability by dynamically adjusting external voltage and excellent absorption efficiency. The physical mechanism of the absorption is studied through magnetic components, which depicts the relations between different resonance peaks. The influence of structural parameters on absorption provides a way to optimize the tunable range of absorption. Finally, we prove the good wide-angle adaptability of absorption from 0° to 60° under TM-polarization. The designed absorber could be further designed to achieve multi-band absorption and be applied in medical measure and terahertz stealth fields.

Acknowledgments

We acknowledge the support from the National Natural Science Foundation of China (Nos. 61775050 and 11804073), the Natural Science Foundation of Anhui Province, China (1808085QA21) and Fundamental Research Funds for the Central Universities (PA2019GDZC0098).

References

1. T. R. Globus, D. L. Woolard, T. Khromova, T. W. Crowe, M. Bykhovskaia, B. L. Gelmont, J. Hesler and A. C. Samuels, *J. Bio. Phys.* **29** (2003) 89.
2. S. Yamaguchi, Y. Fukushi, O. Kubota, T. Itsuji, T. Ouchi and S. Yamamoto, *Sci. Rep.* **6** (2016) 30124.
3. S. Kang, Z. Qian, V. Rajaram, S. D. Calisgan, A. Alù and M. Rinaldi, *Adv. Optical Mater.* **7** (2018) 1801236.
4. P. Yu, L. V. Besteiro, Y. Huang, J. Wu, L. Fu, H. H. Tan, C. Jagadish, G. P. Wiederrecht, A. O. Govorov and Z. Wang, *Adv. Optical Mater.* **7** (2018) 1800995.
5. P. Yu, L. V. Besteiro, J. Wu and A. O. Govorov, *Opt. Express* **26** (2018) 20471.
6. R. Xu and Y. Lin, *Opt. Lett.* **43** (2018) 4783.
7. B. Lee and Z. Zhang, *J. Appl. Phys.* **100** (2006) 063529.
8. C. Liu, L. Qi and M. Wu, *Opt. Mater. Express* **8** (2018) 2439.
9. J. Yang, Z. Zhu, J. Zhang, C. Guo, W. Xu, K. Liu, X. Yuan and S. Qin, *Sci. Rep.* **8** (2018) 3239.
10. F. Xiong, J. Zhang, Z. Zhu, X. Yuan and S. Qin, *Sci. Rep.* **5** (2015) 16998.
11. L. Zhao, H. Liu, Z. He and S. Dong, *Opt. Express* **26** (2018) 12838.
12. S. Huang, Z. Xie, W. Chen, J. Lei, F. Wang, K. Liu and L. Li, *Opt. Exp* **26** (2018) 7066.

13. Y. Jiang, H. Zhang, J. Wang, C. Gao, J. Wang and W. Cao, *Opt. Lett.* **43** (2018) 4296.
14. B. Xu, C. Gu, Z. Li, L. Liu and Z. Niu, *IEEE Antennas Propag. Lett.* **13** (2014) 822.
15. X. Huang, X. Zhang, Z. Hu, M. Aqeeli and A. Alburaikan, *IET Microw. Antennas Propag.* **9** (2015) 307.
16. A. Fardoost, F. G. Vanani, A. Amirhosseini and R. Safian, *IEEE Trans. Nanotechnol.* **16** (2017) 68.
17. D. Chen, J. Yang, J. Zhang, J. Huang and Z. Zhang, *Sci. Rep.* **7** (2017) 15836.
18. M. Rahmanzadeh, H. Rajabalipanah and A. Abdolali, *Appl. Opt.* **57** (2018) 959.
19. A. Akhavan, S. Abdolhosseini, H. Ghafoorifard and H. Habibiyan, *J. Lightwave Technol.* **36** (2018) 5593.
20. Z. Bao, J. Wang, Z. D. Hu, A. Balmakou, S. Khakhomov, Y. Tang, and C. Zhang, *Opt. Express* **27** (2019) 31435.
21. J. Wang, L. Yang, Z. Hu, W. He and G. Zheng, *IEEE Photon. Technol. Lett.* **31** (2019) 561.
22. J. Wang, X. Wang, H. Shao, Z. D. Hu, G. Zheng and F. Zhang, *Nanoscale Res. Lett.* **11** (2017) 9.
23. D. U. Yildirim, A. Ghobadi and E. Ozbay, *Sci. Rep.* **8** (2018) 15210.
24. X. Zhu, J. Fu, F. Ding, Y. Jin and A. Wu, *Sci. Rep.* **8** (2018) 15240.
25. X. Zou, G. Zheng, L. Xu, Y. Chen and M. Lai, *Opt. Lett.* **43** (2018) 46.
26. L. A. Falkovsky and S. S. Pershoguba, *Phys. Rev. B* **76** (2007) 153410.
27. L. Huang, G. Hu, C. Deng, Y. Zhu, B. Yun, R. Zhang and Y. Cui, *Opt. Exp* **26** (2018) 29192.
28. H. Meng, L. Wang, G. Liu, X. Xue, Q. Lin and X. Zhai, *Appl. Opt.* **56** (2017) 6022.
29. L. Ju, X. Xie, W. Du, Y. Liu, J. Hao, B. Ma and H. Yang, *Phys. Status Solidi B* **2019** (2018) 1800382.
30. H. Lu, D. Mao, C. Zeng, F. Xiao, D. Yang, T. Mei and J. Zhao, *Opt. Mater. Exp.* **8** (2018) 1058.
31. C. Liu, L. Qi and X. Zhang, *AIP Adv.* **8** (2018) 015301.
32. Y. Ning, Z. Dong, J. Si and X. Deng, *Opt. Exp.* **25** (2017) 32467.
33. H. Huang, H. Xia, W. Xie, Z. Guo, H. Li and D. Xie, *Sci. Rep.* **8** (2018) 4183.
34. T. Liu and S. Kim, *Sci. Rep.* **8** (2018) 13889.
35. D. Wu, C. Liu, Y. Liu, L. Yu, Z. Yu, L. Chen, R. Ma and H. Ye, *Opt. Lett.* **42** (2017) 450.
36. Y. Lu, J. Li, S. Zhang, J. Sun and J. Yao, *Appl. Opt.* **57** (2018) 6269.